Catal Lett (2009) 130:211–216
DOI 10.1007/s10562-009-9865-6

CO Oxidation Catalyzed by Ag/SBA-15 Catalysts Prepared via in situ Reduction: The Influence of Reducing Agents

Dong Tian · Guoping Yong · Ya Dai · Xiangyang Yan · Shaomin Liu

Received: 19 November 2008 / Accepted: 12 January 2009 / Published online: 11 February 2009

Abstract Ag/SBA-15 catalysts have been prepared by means of in situ reduction methods using hexamethylenetetramine and formaldehyde as reducing agents, respectively, and characterized by N_2 adsorption/desorption, XRD, TEM and XPS. Presence of nanoparticles of silver in SBA-15 were confirmed by high angle X-ray diffraction data (peaks between $2\theta = 35$–80°) and XPS, and transmission electron microscopy confirmed the diameter of the nanoparticles. When hexamethylenetetramine was used as reducing agent, uniform Ag nanoparticles inside the channels were formed, and diameter of nanoparticles is found to be $\sim$6.0 nm which is coincident with channel diameter of SBA-15. The catalysts were subjected to CO oxidation in a flow reactor at atmospheric pressure and temperatures up to 300 °C. Studies revealed that catalysts prepared with different reducing agents strongly influence their catalytic performance in the CO oxidation, what prepared with hexamethylenetetramine as mild reducing reagent shows a certain low temperature catalytic activity.

D. Tian · G. Yong (✉) · X. Yan · S. Liu (✉)
Department of Chemistry, University of Science and Technology of China, 230026 Hefei, China
e-mail: gpyong@ustc.edu.cn

S. Liu
e-mail: liusm@ustc.edu.cn

D. Tian
Department of Chemistry, Huainan Normal College, 232001 Huainan, China

Y. Dai
Technology Center, China Tobacco ChuanYu Industrial Corporation, 610017 Chengdou, China

Keywords Ag/SBA-15 catalysts · CO oxidation · Silver nanoparticles · In situ reduction

1 Introduction

The low-temperature catalytic oxidation of CO has become an important research topic over the years due to its many potential application fields [1, 2]. Precious metal catalysts, such as Au-based catalysts [3–7], have been widely studied and show high catalytic activities for CO oxidation. Comparatively, much less information is currently available on the performance of Ag-based catalysts in the same reaction [8–10]. Also, it seems that little attention has been devoted to the CO oxidation over mesoporous silica supported Ag nanoparticles [11]. According to their narrow pore size distribution, high specific surface area and large pore volume, SBA-15 mesoporous silica materials are a promising candidate for catalyst support. Moreover, SBA-15 possesses a high specific surface area (600–1,000 m^2/g) and consists of a hexagonal array of uniform tubular channels with tunable pore diameter in the range of 5–30 nm. SBA-15 is therefore one of the most attractive silica host-material for metal or metal oxide nanoparticles.

Up to date, there was certain success with the formation of mesoporous silica supported silver nanoparticles or nanowires by using the different reduction methods [11–16], however, to the best of our knowledge, hexamethylenetetramine (HMTA) was used as mild and effective reducing agent for preparation mesoporous silica supported silver nanoparticles hasn't been reported. As reported previously [17–19], at elevated temperature, HMTA can be hydrolyzed in aqueous solution and slowly generate ammonium hydroxide and formaldehyde, as a result, metal nanoparticles can be prepared via reduction of

metal precursor salt with in situ slowly generating formaldehyde [18].

The present work aims at preparing active Ag/SBA-15 catalyst for CO oxidation via in situ reduction method using HMTA as mild and efficient reducing agent. The catalytic performance of this material was compared with Ag/SBA-15 catalyst prepared by in situ reduction using formaldehyde as reducing agent. It will be demonstrated that the former exhibits initially catalytic activity for CO oxidation at slightly above room temperature.

2 Experimental

2.1 Catalyst Preparation

Supported Ag/SBA-15 catalysts were synthesized via in situ reduction methods by using HMTA and formaldehyde as reducing agent, respectively. When HMTA was used as reducing agent, Ag/SBA-15(H) was prepared as follows: 1 g triblock copolymer pluronic P123 was dissolved in 30 mL water to get a clear solution. Thereafter, 3 g nitric acid was added, and the solution was stirred at 35 °C for 1 h. Then, 0.125 g $AgNO_3$ and 0.35 g HMTA were added, and the resulting mixture was stirred for another 3 h at 35 °C while darkening. After 2.13 g TEOS was added and continuously stirred at 35 °C for 20 h while darkening, the mixture was crystallized at 100 °C for 48 h under static and darkening conditions. The resulting solid was filtered, washed several times with water and ethanol, and then dried 10 h at 50 °C under vacuum condition. The molar gel composition was 1TEOS/163H_2O/3.2HNO_3/0.017P123/0.072$AgNO_3$/0.24HMTA. Finally, the solid was calcined in air at 550 °C (heating rate 2 °C/min) for 5 h. When formaldehyde was used as reducing agent, Ag/SBA-15(F) with an equimolar gel composition was prepared following the same procedure. The molar gel composition for Ag/SBA-15(F) was 1TEOS/163H_2O/3.2HNO_3/0.017P123/0.072AgNO_3/0.24 formaldehyde. For comparison, pure siliceous SBA-15 was also synthesized according to literature [20].

2.2 Catalyst Characterization

Powder X-ray diffraction (PXRD) patterns were recorded on a Philips X'Pert PRO SUPER diffractometer operating with nickel-filtered Cu-Kα radiation. X-ray photoeletron spectroscopy (XPS) measurements were performed on a ESCALAB 250 high performance electron spectrometer using monochromatized Al Kα excitation source ($h\nu$ = 1486.6 eV).Transmission electron micrographs (TEM) were taken on a JEOL-2010 electron microscope operating at 200 kV, and sizes of the Ag nanoparticles were estimated from the TEM images. N_2 adsorption/desorption isotherms were obtained at −196 °C on an Omnisorp 100CX instrument. The pore size distributions were determined from the desorption branch of the isotherms with the Barrett–Joyner–Halenda (BJH) method, and the specific surface area values were calculated using the BET model. The amounts of Ag loaded in mesoporous silicas were determined by Atomscan Advantage inductively coupled high frequency plasma atomic emission spectrometry (ICP-AES).

2.3 Catalytic Activity Measurements

The catalytic activity and stability of the SBA-15 supported nanosilver catalysts in CO oxidation were evaluated on a small fixed-bed microreactor operating under atmospheric pressure and an online GC using 50 mg sample. The flow rate of the feed gas was 30 mL/min. The analysis of the effluent gas was tested with an online FuLi9790 model gas chromatograph equipped with a Molecular Sieve 3 Å column and a thermal conductivity detector (TCD). The catalysts were directly exposed to reaction gas containing 2.5% (v/v) CO, 10% (v/v) O_2, and 87.5% (v/v) N_2. The conversion of CO was calculated from the change in CO concentration in the inlet and outlet gases.

3 Results and Discussion

Figure 1 shows low angle X-ray diffraction patterns of calcined SBA-15, Ag/SBA-15(H) and Ag/SBA-15(F). The peak appearing at the low angle of $2\theta \approx 1°$ corresponds to (100) plane of SBA-15, indicating an ordered pore structure which can be attributed to two dimensional hexagonal lattice of SBA-15 [20]. All three samples also show well-resolved (110) and (200) diffraction peaks, indicating no substantial changes after the modification with Ag. However, after loading Ag, the (100) peaks are shifted to higher 2θ values, which are attributed to the network shrinkage (the a_0 parameters of SBA-15, Ag/SBA-15(H) and Ag/SBA-15(F) are 11.55, 10.59 and 9.88 nm, respectively). $AgNO_3$ can be adsorbed on the EO moiety surfaces to form a complex with the micelles formed by P123 in aqueous solution, which possibly resulted in the long hydrophobic chain shrinkage of P123 [14], giving rise to the network shrinkage of Ag/SBA-15(H) and Ag/SBA-15(F). On the other hand, Ag^+ can form complex with HMTA, which decreased its complex with P123, as a result, the lattice contraction of Ag/SBA-15(H) is smaller than Ag/SBA-15(F). Further, the formation of silver nanoparticles in SBA-15 is confirmed by high angle X-ray diffraction data (2θ = 35–80°) (Fig. 2a). Four intense diffraction peaks, corresponding to the (111), (200), (220) and (311) lattice planes of the cubic structure of Ag, confirm the formation of crystalline silver. According to the scherrer equation, the

average crystallite size of silver nanoparticles for Ag/SBA-15(H) and Ag/SBA-15(F) is about 9 and 20 nm, respectively. The broad peak between $15° \leq 2\theta \leq 35°$ corresponds to the mesoporous silica. To further prove the state of silver incorporated into SBA-15, XPS spectra were taken. It is found that the binding energy of silver $3d_{5/2}$ electron is 368.23 and 368.44 eV, respectively. The binding energy is similar to the value of 368.20 eV for Ag $3d_{5/2}$ of bulk silver [21].

It is noteworthy that when formaldehyde was used as reducing agent, Ag/SBA-15(F) exhibits obvious intense diffraction peaks typical of metallic silver (Fig. 2a), implying larger silver crystallites possibly comes from more violent reduction reaction of formaldehyde. The violent reduction can also result in agglomeration of silver nanoparticles. Whereas, when HMTA was used as reducing agent, silver ions probably existed as amine complex, which was more stable than free silver ions, therefore, the reduction of such silver complex by in situ generating formaldehyde should be slow, giving rise to more fine and uniform silver crystallites (relatively weak diffraction peaks), as demonstrated by XRD patterns (Fig. 2a). Interestingly, in present work, Ag nanoparticles were not formed by thermally decomposing $AgNO_3$ to Ag under calcination condition (550 °C), but reduced by in situ reaction during crystallized procedure (100 °C for 48 h), that can be confirmed by XRD patterns of the as-synthesized Ag/SBA-15 samples without calcination (Fig. 2b). Figure 2b also shows that Ag nanoparticles reduced by formaldehyde possesses more intense diffraction peaks, implying that large silver crystallites result from not high calcination temperature [7], but violent reduction condition of formaldehyde.

As shown in Fig. 3, the TEM images of Ag/SBA-15(H) and Ag/SBA-15(F) show hexagonal arrays of mesoporous

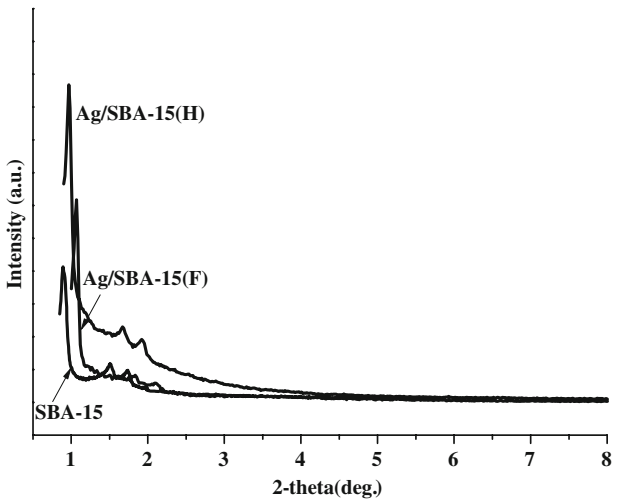

Fig. 1 Small angle XRD patterns of pristine SBA-15 and Ag/SBA-15

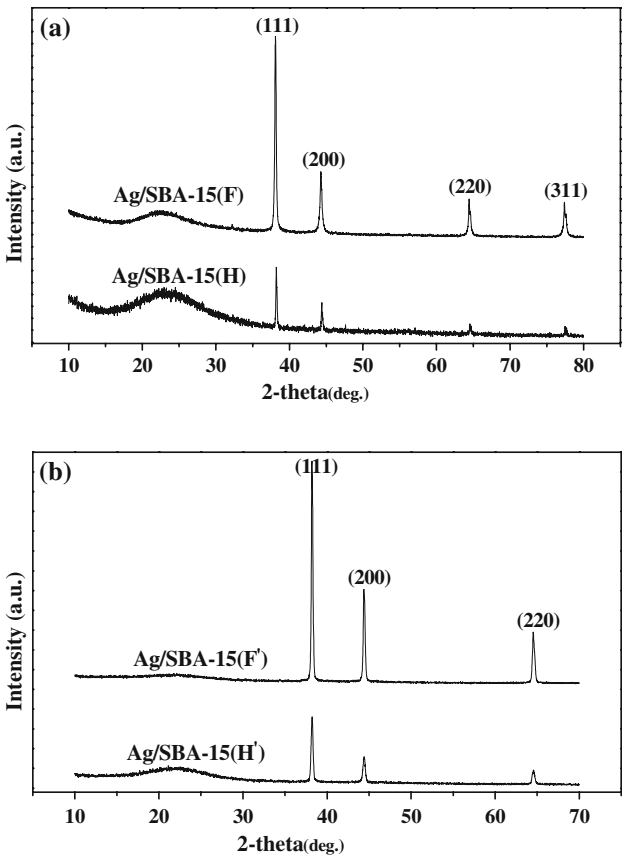

Fig. 2 XRD patterns at high angle of **a** calcined Ag/SBA-15 and **b** as-synthesized Ag/SBA-15

channels. A homogeneous dispersion of Ag nanoparticles inside Ag/SBA-15(H) channels can be clearly observed (Fig. 3a). In contrast, the larger agglomerations of Ag nanoparticles exist outside Ag/SBA-15(F) channels as illustrated by obviously dark areas (the bright areas corresponding to the silica walls), as shown in Fig. 3b. One can also observe only a few Ag nanoparticles exist inside Ag/SBA-15(F) channels. The Ag nanoparticles in Ag/SBA-15(H) exhibit a relatively narrow size distribution (average 6 nm). The smaller and uniform nanoparticles existed in Ag/SBA-15(H) were probably due to the size confinement effect of SBA-15 pore channels (average 7 nm calculated by the BJH method) and the low nucleation rate which were slowed down to agglomeration because of the slow reduction by in situ generating formaldehyde from HMTA. Broadening of the nanoparticle size distribution for Ag/SBA-15(F) (4–23 nm) may be the consequence of agglomeration. The new silver nucleus were fast formed due to violent reduction by formaldehyde, as a result, silver nanoparticles had a good chance to aggregate. The present results demonstrate that more homogeneous dispersion of Ag nanoparticles (average 6 nm) can be achieved, when prepared by more mild and slow reduction with in situ generating formaldehyde from HMTA.

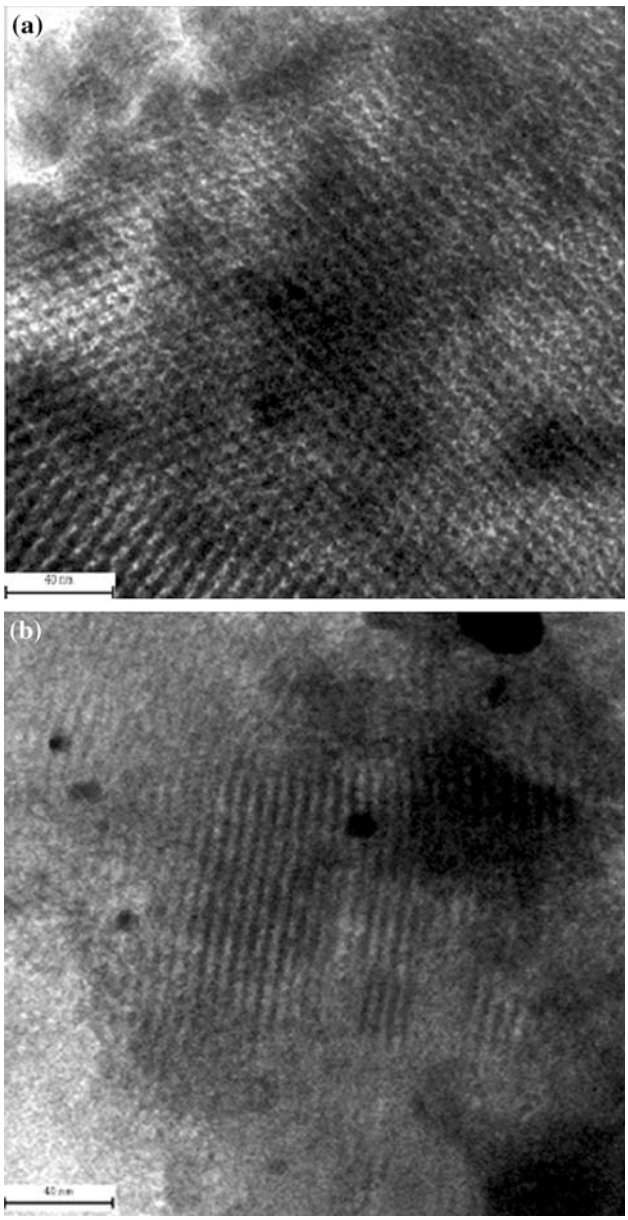

Fig. 3 TEM images of the calcined **a** Ag/SBA-15(H) and **b** Ag/SBA-15(F). The *bright areas* correspond to the silica walls and the *dark areas* to the Ag nanoparticles

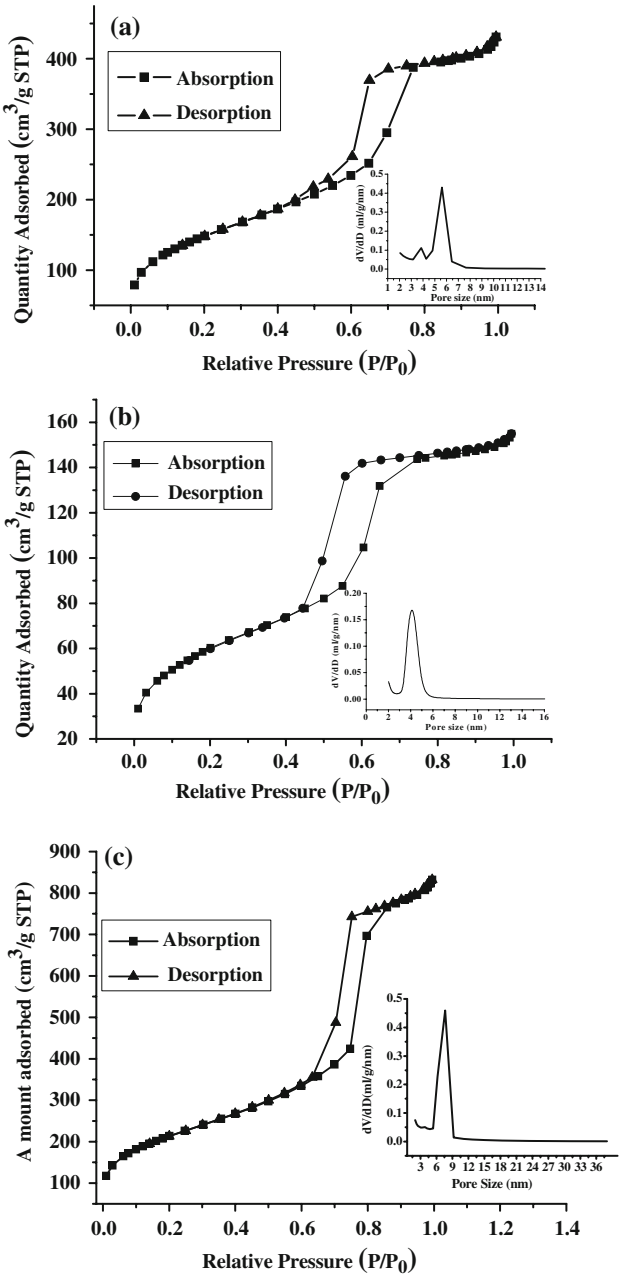

Fig. 4 The nitrogen adsorption/desorption isotherms and pore size distribution curves (*insert*) of **a** Ag/SBA-15(H), **b** Ag/SBA-15(F) and **c** SBA-15

As shown in Fig. 4, SBA-15, Ag/SBA-15(H) and Ag/SBA-15(F) exhibit similar N_2 adsorption/desorption isotherms of type IV with a H_1 hystersis loops following the IUPAC classification [22]. The profiles are a characteristic of mesoporous materials having cylindrical channels. Three well-distinguished regions of the adsorption isotherms (Fig. 4) are obvious: (1) monolayer multilayer adsorption ($P/P_0 = 0$–0.5); (2) capillary condensation ($P/P_0 = 0.5$–0.8) and (3) multilayer adsorption on the outer surface ($P/P_0 = 0.8$–1.0). A sharp inflection in the relative pressure (P/P_0) between 0.5 and 0.8 corresponds to capillary condensation within uniform mesopores, and is a function of the pore diameter. The uniform pore size distribution is demonstrated by the sharpness of this step and displayed in the insets of Fig. 4a–c. The surface areas of Ag/SBA-15(H) (525 m^2/g) and Ag/SBA-15(F) (220 m^2/g) are lower than SBA-15 (773 m^2/g), which can be attributed to the agglomeration of Ag nanoparticles, that partly block the pore space of mesoporous channels [23]. It is important to note that surface area of Ag/SBA-15(F) is sufficiently decreased,

demonstrating more obvious agglomeration of Ag nanoparticles in Ag/SBA-15(F) envelop its pore space.

Both Ag/SBA-15(H) and Ag/SBA-15(F) catalysts exhibit different catalytic behavior in CO oxidation, as shown in Fig. 5a which shows the conversion of CO over Ag/SBA-15 catalysts as a function of the reaction temperature. Conversion of CO for Ag/SBA-15(F) catalyst maintains at a very low level over temperature range of 25–150 °C, implying it is catalytically inactive for the CO oxidation until 150 °C, although several studies indicated that CO can be oxidized over silver even below room temperature [24]. However, CO can be oxidized over Ag/SBA-15(H) catalyst even at slightly above room temperature (CO conversion of 8% at 40 °C, 16% at 75 °C and 23% at 150 °C), showing conversion increases with an increase of reaction temperature. The reason for this initially catalytic activity is probably ascribed to more homogeneous dispersion of Ag nanoparticles in SBA-15 as shown in TEM image (Fig. 3a). Interestingly, the CO conversion curve of Ag/SBA-15(H) exhibits two conversion steps. The first, the CO conversion between 25 and 125 °C, is probably ascribed to the catalysis of the Ag nanoparticles outside channels. The second step, at a high relative temperature (125–200 °C), possibly corresponds to catalysis of the Ag nanoparticles inside channels. As for Ag/SBA-15(F) system, inactivity can possibly result from the agglomeration of Ag nanoparticles (maximum size of 23 nm). It is also worth mentioning that the agglomeration of Ag nanoparticles significantly decreases BET surface area, giving rise to lessen of oxygen adsorption, and as a result, decreases catalytic activity. Ag/SBA-15(H) shows lower temperature catalytic performance, becoming active at slightly above room temperature and reaching full conversion at 230 °C. Whereas, Ag/SBA-15(F) becomes active until 150 °C, and achieves a 100% CO conversion over 270 °C. Although the amount of Ag loaded in Ag/SBA-15(H) (5.28 wt%) is almost the same as Ag/SBA-15(F) (5.16 wt%), Ag/SBA-15(H) catalyst, consisting of more uniform and smaller Ag nanoparticles (average 6 nm), shows more excellent catalytic performance for CO oxidation [25]. The catalytic stability of Ag/SBA-15(H) catalyst was measured. When the reactor temperature was maintained at 150 °C for 3 h, and then up to 240 °C (heating rate 5 °C/min) and maintained at 240 °C for another 3 h, the catalytic activity was maintained over 6 h testing period for two different temperatures (Fig. 5b). These results demonstrate Ag/SBA-15(H) catalyst possesses very highly catalytic stability.

The observed Ag nanoparticle size—catalytic activity relation in the CO oxidation may attribute to the fine and non-aggregated Ag nanoparticles that are more chemically active. Further, investigations are required to reveal the influence of the Ag loading amounts on the catalytic

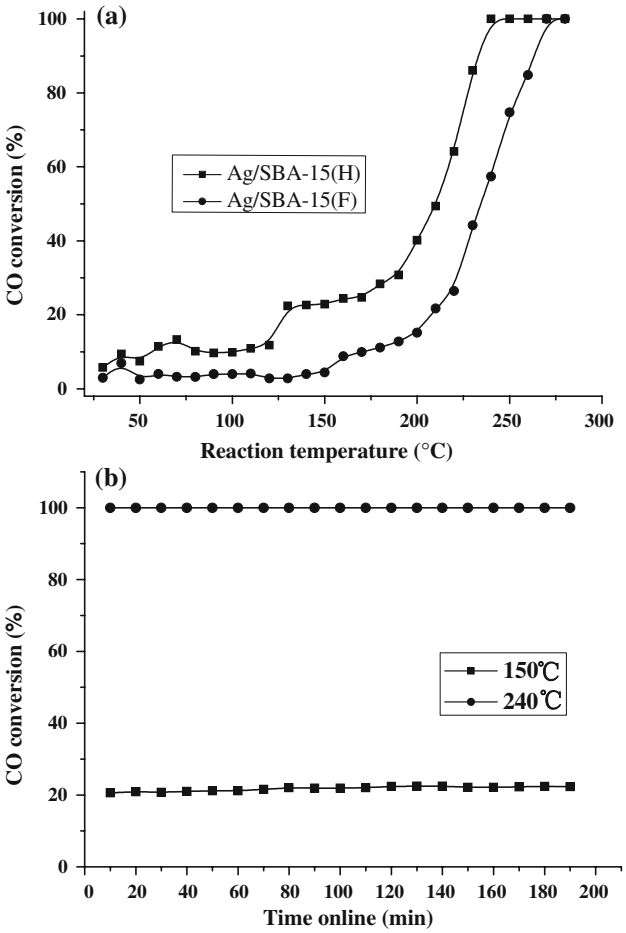

Fig. 5 The catalytic **a** activity and **b** stability measurement of CO conversion over Ag/SBA-15 catalysts

performance of Ag/mesoporous silicas prepared by HMTA, which are undergoing in our laboratory. Also, some organic reaction catalyzed by such Ag/mesoporous silicas will be undergone in our laboratory.

4 Conclusions

We have successfully prepared Ag/SBA-15(H) catalyst via in situ reduction method with mild and efficient reducing agent HMTA, whereas, in situ reduction with formaldehyde leads to the agglomeration of Ag nanoparticles. Utilizing the HMTA as reducing agent, Ag nanoparticles of ~6 nm coincident with channel diameter of SBA-15 were formed and confirmed by TEM. This may be due to low nucleation rate and the size confinement of pore channels. These catalysts behave differently in CO oxidation. Ag/SBA-15(H) catalyst shows a certain low temperature catalytic activity, which results from its uniform and small Ag nanoparticles. Study also reveals strong influence of the reducing agent on the performance of catalysts in the CO oxidation.

Acknowledgments This work was financially supported by the National Natural Science Foundation of China (grant 20872135) and China National Tobacco Corporation.

References

1. Shelef M, McCabe RW (2000) Catal Today 62:35
2. Kim DH, Lim MS (2002) Appl Catal A Gen 224:27
3. Jia ML, Shen YN, Li CY, Bao ZRGT, Sheng SS (2005) Catal Lett 99:235
4. Chiang CW, Wang AQ, Wan BZ, Mou CY (2005) J Phys Chem B 109:18042
5. Budroni G, Corma A (2006) Angew Chem Int Ed 45:3328
6. Ruszel M, Grzybowska B, Łaniecki M, Wójtowski M (2007) Catal Commun 8:1284
7. Tsoncheva T, Ivanova L, Lotz AR, Smått JH, Dimitrov M, Paneva D, Mitov I, Linden M, Minchev C, Fröba M (2007) Catal Commun 8:1573
8. Hu RR, Xie LY, Ding S, Hou J, Cheng Y, Wang DZ (2008) Catal Today 131:513
9. Jin L, Qian K, Jiang ZQ, Huang WX (2007) J Mol Catal A Chem 274:95
10. Frey K, Iablokov V, Melaet G, Guczi L, Kruse N (2008) Catal Lett 124:74
11. Gac W, Derylo-Marczewska A, Pasieczna-Patkowska S, Popivnyak N, Zukocinski G (2007) J Mol Catal A Chem 268:15
12. Huang MH, Choudrey A, Yang PD (2000) Chem Commun 1063
13. Hornebecq V, Antonietti M, Cardinal T, Treguer-Delapierre M (2003) Chem Mater 15:1993
14. Zhu WP, Han YC, An LJ (2005) Microporous Mesoporous Mater 80:221
15. Sun JM, Ma D, Zhang H, Liu XM, Han XW, Bao XH, Weinberg G, Pfänder N, Su DS (2006) J Am Chem Soc 128:15756
16. Plyuto Y, Berquier JM, Jacquiod C, Ricolleau C (1999) Chem Commun 1653
17. Blazevic N, Kolbach D (1979) Synthesis 161
18. Zhi LJ, Zhao T, Yu YZ (2002) Scr Mater 47:875
19. Govender K, Boyle DS, Kenway PB, O'Brien P (2004) J Mater Chem 14:2575
20. Zhao D, Feng J, Huo Q, Melosh N, Fredrickson GH, Chmelka BF, Stucky GD (1998) Science 279:548
21. Citrin PH, Wertheim GK, Baer T (1983) Phys Rev B 27:3160
22. Sing KSW, Everett DH, Haul RAW, Mosenu L, Pierotti RA, Rouquerol J, Siemieniewska T (1985) Pure Appl Chem 57:603
23. Zhao XG, Shi JL, Hu B, Zhang LX, Hua ZL (2004) Mater Lett 58:2152
24. Barth JV, Zambelli T (2002) Surf Sci 513:359
25. Qu Z, Huang W, Cheng M, Bao X (2005) J Phys Chem B 109: 15842